Supplementary Information

Details of biochar characterization

The bulk elemental composition of the pyrochars and hydrochars was analyzed on an analyzer (EA3000, Italy). The ash content was calculated by mass difference. The surface elemental composition and functional group distribution were analyzed using an ESCALAB Mark II spectrometer (VG Scientific Ltd., UK) with a monochromated Al Kα X-ray source operated at 200 W. The survey spectrum and the high-energy resolution scans of C1s region from 280-300 eV were collected and analyzed using the XPSpeak4.1 software. Chemical bond analysis of the C was conducted by deconvoluting the high-resolution C1s scans into four components: C-C bonds (284.9 eV), C-O bonds (286.5 eV), C=O bonds (287.9 eV), and COO bonds (289.4 eV) (Jin et al., 2017). The surface functional group distributions were examined using a FT-IR spectrophotometer (JASCO FTIR 410, Japan). The specific surface area (SA) and pore size distribution of the biochars were analyzed using N_2 adsorption at 77 K using an adsorption instrument (TriStarII, Micromeritics Company, USA). The surface morphologies of the biochars were obtained from a scanning electron microscope (SEM) (Hitachi S4800, Japan).

Details of data analysis

The pseudo-first-order order (Eq. (1)), pseudo-second-order (Eq. (2)), and intra-particle diffusion (Eq. (3)) models were used to simulate the sorption kinetic process.

$$\ln(q_e - q_t) = \ln q_e - k_1 t \quad (1)$$

$$t/q_t = 1/(k_2 \times q_e^2) + t/q_e = 1/v_0 + t/q_e \quad (2)$$

$$q_t = k_d t^{1/2} + c \quad (3)$$

where q_t (μg/g) is the solid-phase concentration of OPFRs adsorbed by biochars at time t, k_1 (h^{-1}) and k_2

(g/μg/h) are the pseudo-first-order and pseudo-second-order kinetic rate constants, respectively, v_0 (μg/g/h) is the initial sorption rate of OPFRs on the biochars. k_d (μg/g/h$^{0.5}$) is the intraparticle diffusion rate constant and c (μg/g) is the boundary layer thickness coefficient.

The sorption isotherms of the OPFRs by the biochars were fitted with Langmuir (Eq. (4)) and Freundlich (Eq. (5)) models:

$$q_e = \frac{Q_{\max} K_L C_e}{1 + K_L C_e} \quad (4)$$

where Q_{max} (μg/g) is the maximal amount of OPFRs sorbed on the biochars, and K_L (L/mmol) represents the Langmuir adsorption constant.

$$\log q_e = \log K_F + n \log C_e \quad (5)$$

where K_F ((μg /g)/(μg /L)^n) is the Freundlich affinity coefficient, and parameter n indicates the nonlinearity of sorption isotherm.

Reference

Jin, J., Sun, K., Wang, Z., Yang, Y., Han, L., Xing, B. (2017). Characterization and phenanthrene sorption of natural and pyrogenic organic matter fractions. Environ. Sci. Technol. 51(5), 2635-2642

Table S1 Selected physicochemical properties of triphenyl phosphate (TPhP) and triphenylphosphine oxide (TPPO)

Chemicals	Chemical structure	MF	Diameter (nm)[a]	M (g/mol)	ρ (g/cm^3)	logK_{ow}[b]	C_S[b] (mg/L)	HD	HA	HB	BCF[b]
TPhP	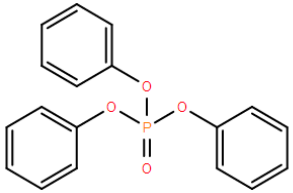	$(C_6H_5O)_3P=O$	1.14	326	1.21	4.59	1.9	0	4	4	113.3
TPPO	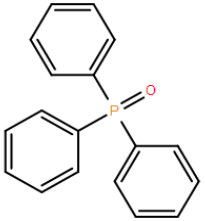	$(C_6H_5)_3P=O$	0.98	278	1.17	2.87	2100	0	1	1	30.1

[a] The maximum diameters of TPhP and TPPO with minimum energy (calculated using Gaussian 09 software).

[b] Data from Wang, et al., 2018; MF, molecular formula; LogK_{ow}, octanol-water partition constant; C_S, water solubility; HD, hydrogen bonding donor; HA, hydrogen bonding acceptor; HB, hydrogen bond-forming ability; BCF, bioconcentration factor.

Table S2 Surface functional groups from the XPS spectra of the rice straw-derived hydrochar and pyrochars.

Samples	C-C (%)	C-O (%)	C=O (%)	COO (%)	Surface polar C (%) [a]
HRS200	52.6	34.8	12.1	0.5	47.4
PRS300	73.3	19.5	6.4	0.9	26.7
PRS450	70.6	27.3	0.0	2.1	29.4
PRS600	80.1	10.6	8.7	0.7	19.9

[a] Surface polar C = (C-O) + (C=O) + (COO).

Note that HRS200 represents rice straw-derived hydrochar; and PRS300, PRS450, and PRS600 represent rice straw-derived pyrochars produced at 300, 450, and 600 ℃, respectively.

Table S3 The parameters of pseudo-first-order, pseudo-second-order, and intra-particle diffusion models of triphenyl phosphate (TPhP) and triphenylphosphine oxide (TPPO) on the biochars.

Samples	Pseudo-first-order [a]			Pseudo-second-order [b]				Intra-particle diffusion parameter [c]		
	q_e (μg/g)	k_1 (h^{-1})	R^2	v_0 (μg/g/h)	k_2 (g/μg/h)	q_e (μg/g)	R^2	k_d (μg/g/$h^{0.5}$)	c (μg/g)	R^2
					TPhP					
PRS300	6290.9	0.17	0.727	2057.8	4.6×10^{-5}	6708.7	0.998	728.0	1814.2	0.903
PRS450	6315.7	0.99	0.635	2210.2	4.0×10^{-5}	7393.1	0.999	503.3	2130.6	0.919
PRS600	8590.8	2.17	0.664	12320.5	1.5×10^{-4}	9087.0	1.000	429.3	6326.3	0.880
					TPPO					
HRS200	118.4	1.62	0.238	48.5	2.3×10^{-3}	144.7	0.999	7.8	72.4	0.994
PRS450	353.1	3.63	0.199	303.0	2.0×10^{-3}	392.2	1.000	11.4	290.0	0.994

[a] Pseudo-first-order model: $\ln(q_e - q_t) = \ln q_e - k_1 t$.

[b] Pseudo-second-order model: $t/q_t = 1/(k_2 \times q_e^2) + t/q_e = 1/v_0 + t/q_e$.

[c] Intra-particle diffusion model: $q_t = k_d t^{1/2} + c$.

Note that HRS200 represents rice straw-derived hydrochar; and PRS300, PRS450, and PRS600 represent rice straw-derived pyrochars produced at 300, 450, and 600 ℃, respectively.

Table S4 Langmuir isotherm parameters of triphenyl phosphate (TPhP) and triphenylphosphine oxide (TPPO) on the biochars.

Samples	Langmuir			
	N^a	K_L (L/mg)	Q_{max} (mg/g)	R^2
		TPhP		
PRS300	14	5.73	9.0	0.976
PRS450	16	7.27	10.0	0.975
PRS600	14	11.9	10.1	0.987
		TPPO		
HRS200	16	0.020	6.4	0.989
PRS300	14	0.019	8.7	0.987
PRS450	16	0.037	10.9	0.991
PRS600	14	0.047	11.2	0.969

[a] Number of data.

Note that HRS200 represents rice straw-derived hydrochar; and PRS300, PRS450, and PRS600 represent rice straw-derived pyrochars produced at 300, 450, and 600 ℃, respectively.

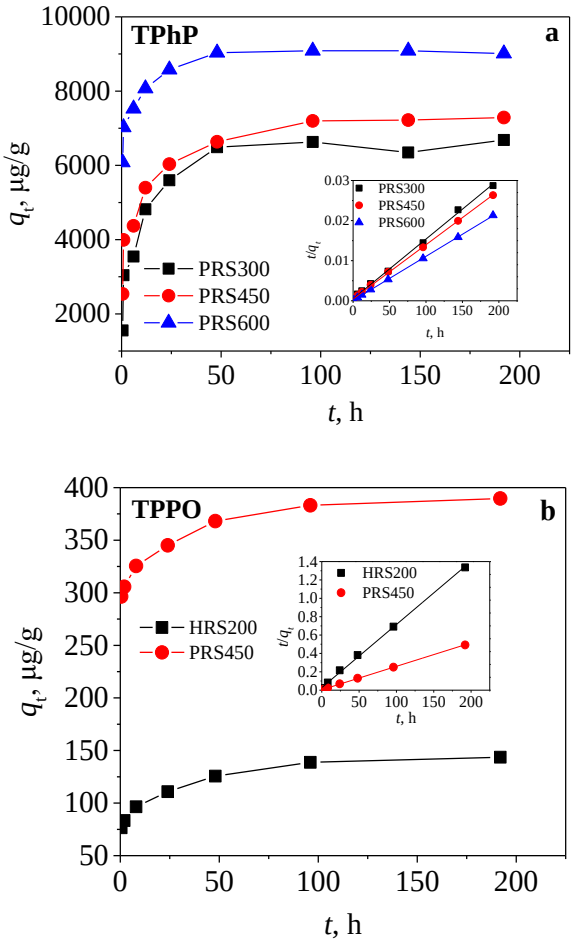

Figure S1. Sorption kinetics of triphenyl phosphate (TPhP) (a) and triphenylphosphine oxide (TPPO) (b) on the hydrochar (HRS200) and pyrochars produced at 300 (PRS300), 450 (PRS450), and 600 (PRS600) ℃; inset is the pseudo-second-order kinetic plots of TPhP and TPPO.

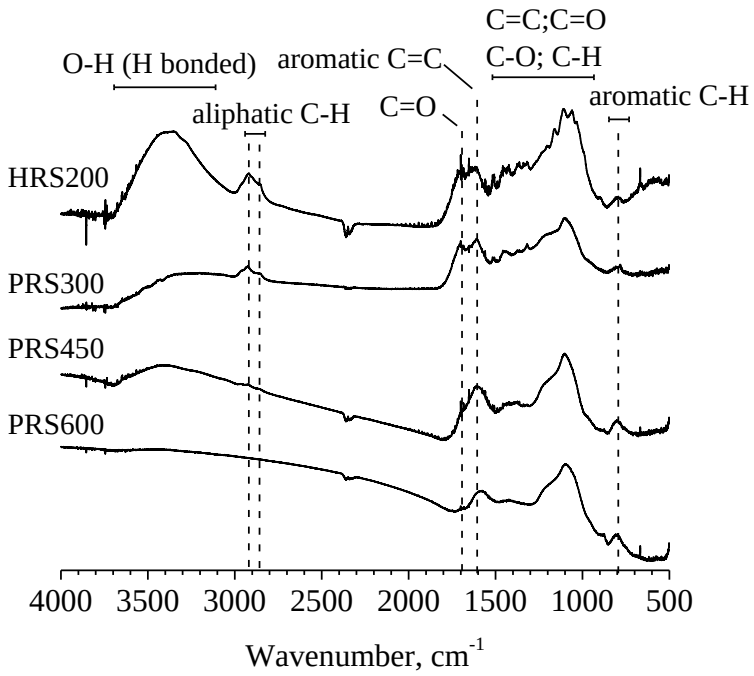

Figure S2. Stacked ATR FT-IR spectra of the hydrochar (HRS200) and pyrochars produced at 300 (PRS300), 450 (PRS450), and 600 (PRS600) ℃.

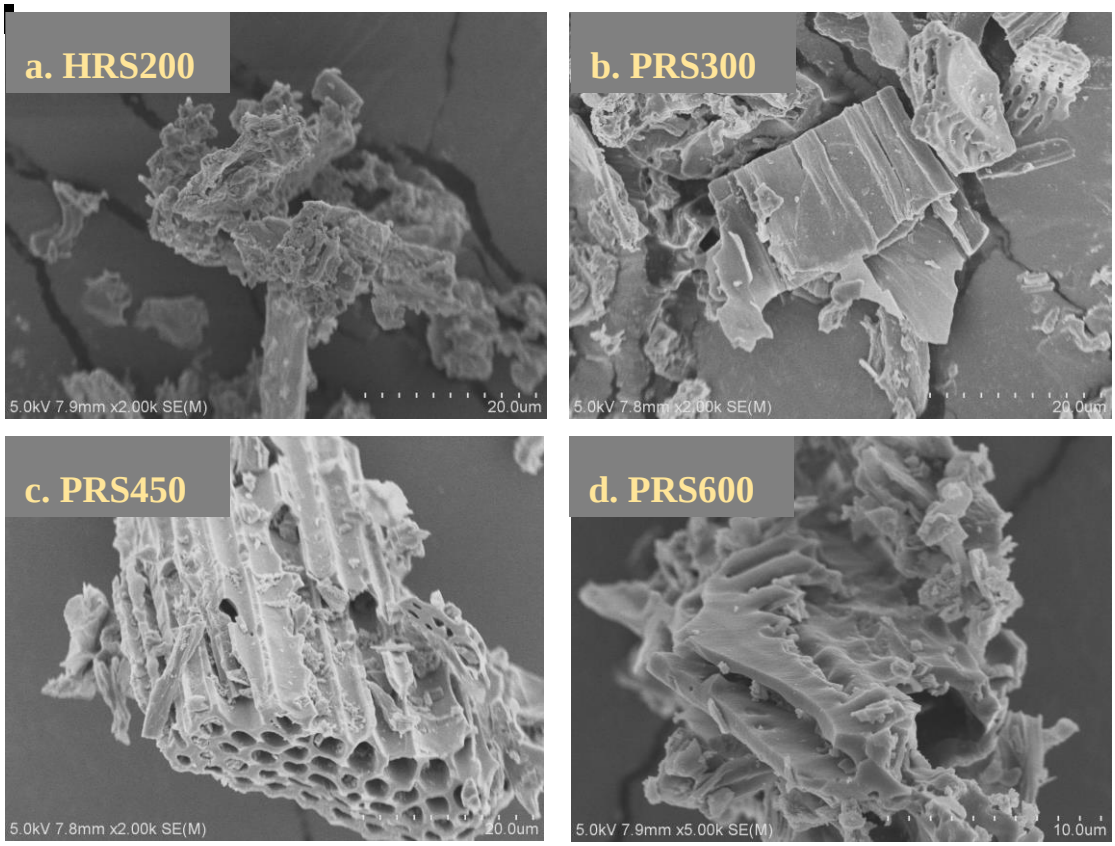

Figure S3. Scanning electron microscope (SEM) images of the hydrochar (HRS200) (a) and pyrochars produced at 300 (PRS300) (b), 450 (PRS450) (c), and 600 (PRS600) ℃ (d).

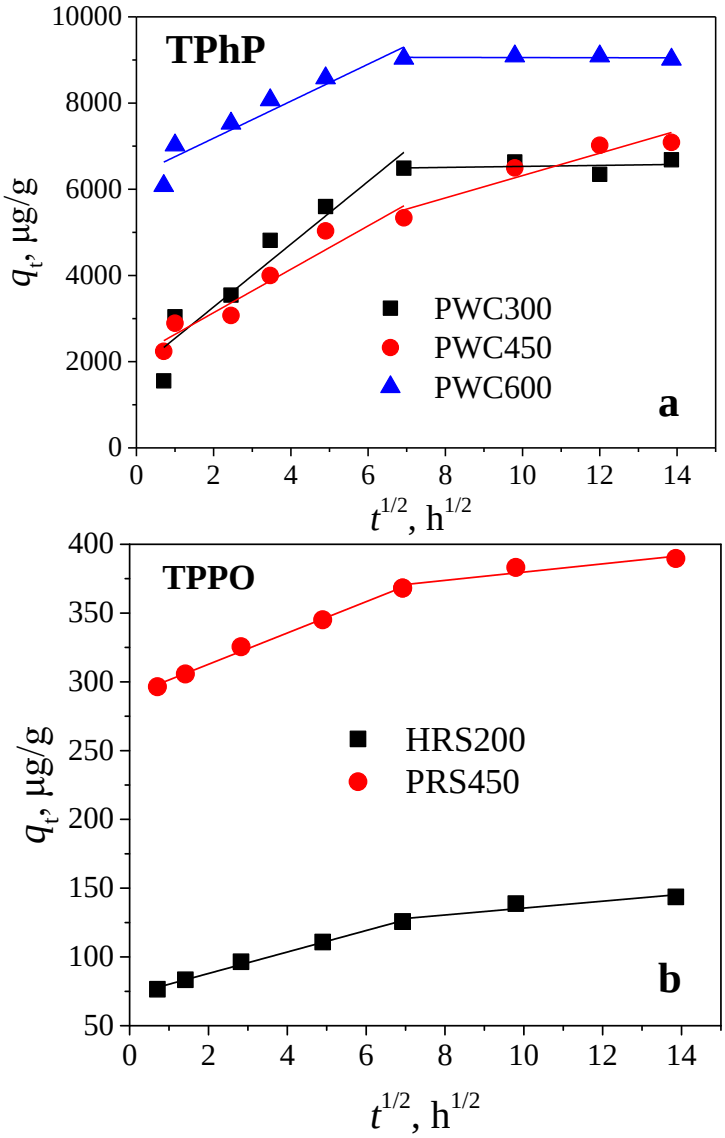

Figure S4. The intra-particle diffusion kinetic plots of triphenyl phosphate (TPhP) (a) and triphenylphosphine oxide (TPPO) (b) on the hydrochar (HRS200) and pyrochars produced at 300 (PRS300), 450 (PRS450), and 600 (PRS600) ℃.

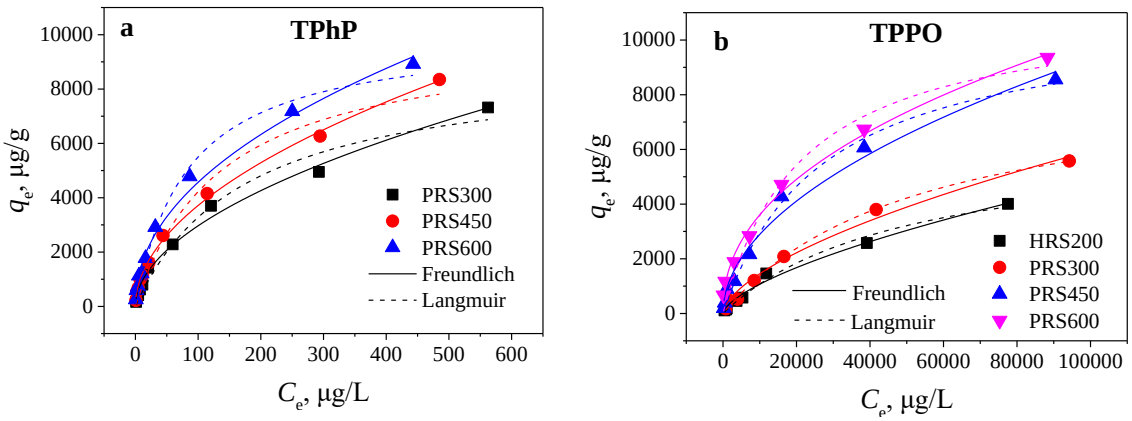

Figure S5. The sorption isotherms of triphenyl phosphate (TPhP) (a) and triphenylphosphine oxide (TPPO) (b) by the hydrochar (HRS200) and pyrochars produced at 300 (PRS300), 450 (PRS450), and 600 (PRS600) ℃.

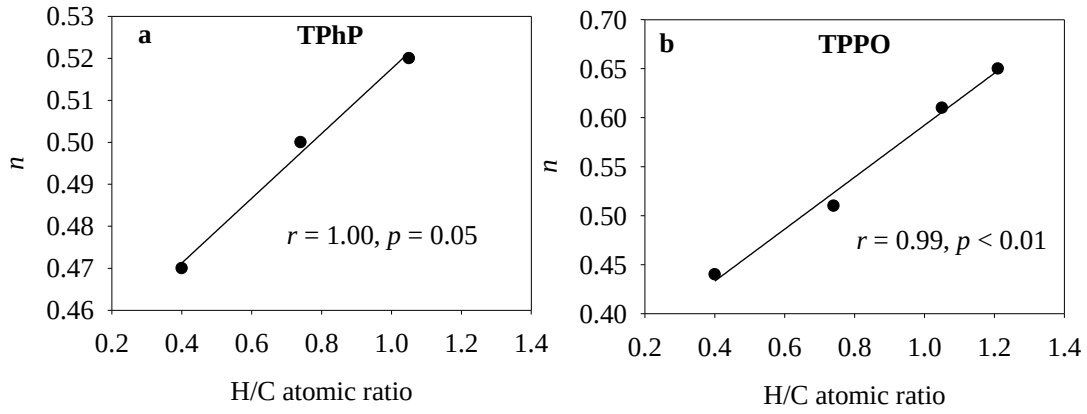

Figure S6. Correlation between the nonlinearity values of triphenyl phosphate (TPhP) (a) and triphenylphosphine oxide (TPPO) (b) by the biochars and their H/C atomic ratios.